25th ABCM International Congress of Mechanical Engineering
October 20-25, 2019, Uberlândia, MG, Brazil

COB-2019-0708
INCOMPRESSIBLE FLOWS BIFURCATION PHENOMENA IN SYMMETRIC CHANNELS

Adyllyson Heverton Gomes do Nascimento
University of Campinas (UNICAMP), School of Mechanical Engineering, Department of Energy, 13083-970 Campinas, SP, Brazil
adyllyson@outlook.com

Gustavo Silva Rodrigues
Federal University of Uberlândia (UFU), School of Mechanical Engineering, Fluid Mechanics Laboratory (MFLab), 38400-902 Uberlândia, MG, Brazil
gsrodrigues@ufu.br

José Ricardo Figueiredo
University of Campinas (UNICAMP), School of Mechanical Engineering, Department of Energy, 13083-970 Campinas, SP, Brazil
jrfigue@fem.unicamp.br

Abstract. *This paper presents a numerical study of the incompressible laminar flows bifurcation phenomena in a two-dimensional symmetric sudden expansion. The solution method of the continuity and Navier-Stokes equations for incompressible flows is based on the Eulerian description of the flow. It uses the primitive variables in the divergent form, in the context of the finite volume, with the UNIFAES scheme for the discretization of the spatial derivatives of the advective-diffusive transport equation. The solution method adopts the explicit time integration procedure of the velocity field and uses the Poisson equation for the pressure field. The solution of the Poisson equation is obtained with several iterations per velocity step in order to ensure mass conservation throughout the transient regime. In comparative studies in this context, the almost unknown semi-staggered mesh structure has been highlighted by accuracy, in relation to the traditional staggered and collocated meshes. Like the semi-staggered mesh, the UNIFAES scheme is justly following this path of extensive evaluation, presenting good performance regarding acuity and stability in the most diverse types of problems previously evaluated. The flow in symmetric channels is known to exhibit a stable symmetric solution up to a critical Reynolds number above which symmetry-breaking bifurcation occurs. The present paper has the contribution of presenting new numerical evaluations of the continuity and Navier-Stokes equations, thus extending the scope of the UNIFAES discretization scheme and the semi-staggered mesh, as well as the methodology used to solve the equations. The results of the numerical procedure are compared with experimental and numerical studies available in the literature.*

Keywords: *Numerical Methods, Sudden Expansion, Finite Volume, UNIFAES, Semi-staggered Mesh*

1. INTRODUCTION

In the last decades, a lot of efforts were devoted to the study of incompressible laminar flow over a sudden expansion. Several previous studies investigated the instability mechanisms that govern the flow, and also deserved experimental studies. See, e.g., Durst *et al.* (1974); Cherdron *et al.* (1978); Fearn *et al.* (1990) and Durst *et al.* (1993). For this reason, the flow over a sudden expansion has become a prototypical problem, being vastly used as a test-case for computational codes solving the continuity and Navier-Stokes equations due to geometric simplicity of the Cartesian configuration.

Observations of laminar flows in two-dimensional channels with symmetric expansion have shown that these flows become asymmetric as the Reynolds number increases, including loss of stability of the symmetric solution. The intriguing physics of these flows is explained by the observation that an increase (or decrease) of the velocity near one wall leads to a decrease (or increase) in the pressure. The pressure difference formed across the channel maintains the asymmetry of the flow. This phenomenon of attachment to the surface is called the Coanda effect (Wille and Fernholz, 1965). Complementary numerical computations of the symmetry-breaking bifurcation point by Fearn *et al.* (1990) and linear stability analyses of flows in symmetric channels by Shapira *et al.* (1990), indicate that this observed experimental behavior occurs at a bifurcation problem governed by the continuity and Navier-Stokes equations.

The physical origin of the asymmetry is related to the instability of the shear layer between the main stream and the recirculating flow. The conditions that give rise to the asymmetric flows are in the disturbances generated at the edge of the expansion and that are amplified in the shear layers, as indicated by Cherdron *et al.* (1978). The stability analyses

of Fearn *et al.* (1990) and Shapira *et al.* (1990) showed that the unique, symmetric solution loses its stability at a certain critical Reynolds number beyond which a pair of stable, asymmetric solutions exists. Because the symmetry-breaking point is structurally unstable, Fearn *et al.* (1990) suggest that the transition from the symmetric to the asymmetric flow is not sudden, and that any type of small perturbation in the flow, such as a slight degree of asymmetry in the expansion geometry, can lead to the appearance of asymmetric flows. The dependence of the critical Reynolds number of the symmetry-breaking bifurcation on the expansion ratio was studied numerically by Alleborn *et al.* (1997), Battaglia *et al.* (1997) and Drikakis (1997). The numerical computations of the symmetry-breaking bifurcation point indicated that critical Reynolds number reduces when increasing the expansion ratio.

The methods adopted to find the critical Reynolds number for the symmetry-breaking bifurcation can be divided into three categories: bifurcation analyzes, numerical simulations and experiments. In the bifurcation analysis, linear stability analysis are adopted to identify the exact bifurcation point (Fearn *et al.*, 1990; Shapira *et al.*, 1990; Alleborn *et al.*, 1997). For the other two methods, it is necessary to gradually increase or decrease the Reynolds number to search for the critical point asymptotically. In addition to, the critical Reynolds number is sensitive to small imperfections that are unavoidable, especially in the experimental apparatus (Cherdron *et al.*, 1978). Therefore, it is quite difficult to locate exactly the bifurcation point by these two methods.

In the present paper, the critical Reynolds number was obtained by means of numerical simulations. As mentioned above, this procedure can not reveal the bifurcation point directly. However, the numerical simulations can predict the flow field with some precision on both sides of the critical condition. Thus, an indication of the bifurcation point can be inferred by starting from one symmetric solution and one asymmetric solution, and decreasing the distance between them by computing flows at intermediate Reynolds numbers. Not surprisingly, the results show that the convergence time becomes larger as it approaches the critical Reynolds number, thus leaving some uncertainty in the final value of the critical point. Similar observations were reported by Battaglia *et al.* (1997). Drikakis (1997) mentions the difficulty of fixing the critical Reynolds number, since the results are extremely dependent on the grid resolution.

The present paper provides a numerical study of the incompressible laminar flows bifurcation phenomena in a two-dimensional sudden expansion. The solution method of the continuity and Navier-Stokes equations employs the Eulerian description of the flow, primitive variables on the divergent form, finite volume approach, semi-staggered mesh, UNIFAES scheme for discretization of the spatial derivatives of the advective-diffusive transport equation, explicit procedure for the temporal integration of the velocity field and Poisson equation for pressure.

2. MATHEMATICAL AND NUMERICAL MODEL

The problem of interest concerns the case of incompressible, viscous and laminar two-dimensional flow. Thus, the non-dimensional continuity and Navier-Stokes equations in Cartesian coordinates are:

continuity:

$$\nabla.\mathbf{V} = 0 \tag{1}$$

linear momentum:

$$\frac{\partial \mathbf{V}}{\partial t} = \mathbf{A_V} - \nabla p \tag{2}$$

where the variable $\mathbf{A_V}$ represents the advective and diffusive net fluxes given in divergent form as:

$$\mathbf{A_V} = -\mathrm{Re}\,\nabla.(\mathbf{VV}) + \nabla.(\nabla\mathbf{V}) \tag{3}$$

Here, the spatial coordinates x and y are made non-dimensional based on a characteristic length L_c, the velocity vector $\mathbf{V} = (u, v)$ by a characteristic velocity V_c and time t by $\rho L_c^2/(\mu V_c)$. The Reynolds number is $\mathrm{Re} = \rho V_c L_c/\mu$. The total non-dimensional pressure can be written by the sum of the physical pressure p and the hydrostatic pressure $\rho g z$, made non-dimensional by the factor $\mu V_c/L_c$.

The governing equations are discretized using the finite volume method, by which differential conservation equations, written in divergent form, are integrated over each control volume of the numerical mesh. After integration, the volume integrals of the advection and diffusion terms are transformed into surface integrals by applying the Gauss divergence theorem. These surface integrals are numerically approximated by the sum of the advective-diffusive fluxes multiplied by the respective areas of the control volume faces. In the present paper, the UNIFAES scheme (Figueiredo, 1997) is used for the spatial discretization of the advective-diffusive terms of the transport equations. Recent evaluations of the UNIFAES scheme can be found in Nascimento *et al.* (2018) and Rodrigues *et al.* (2018).

The explicit integration in time employed by Harlow and Welch (1965), through the MAC method for the staggered mesh structure, was one of the first methods to solve the continuity and Navier-Stokes equations for incompressible flows. The method deals with a Poisson equation for pressure for the coupling of velocity and pressure fields. The explicit

time integration method solves numerically the linear momentum transport equations and the Poisson equation for the pressure, the latter being obtained from the linear momentum and continuity discrete equations. The present paper applies the methodology employed by Harlow and Welch (1965), extending its approach to the semi-staggered mesh structure. The methodology employed in the present paper is also used in Rodrigues *et al.* (2019a,b).

The explicit temporal discretization of the linear momentum equations, Eq. (2), are given by:

$$\frac{\mathbf{V}^{n+1}-\mathbf{V}^{n}}{\Delta t}=\mathbf{A}_{\mathbf{V}}^{n}-\nabla p^{n} \tag{4}$$

The Poisson equation for the pressure is obtained numerically by taking the divergent of the linear momentum equations, Eq. (4), and rearranging to yield:

$$\nabla^{2}p^{n}=\nabla.\mathbf{A}_{\mathbf{V}}^{n}-\frac{\nabla.\mathbf{V}^{n+1}-\nabla.\mathbf{V}^{n}}{\Delta t} \tag{5}$$

In the numerical method, a divergence free velocity is required at the next time step, i.e. $\nabla.\mathbf{V}^{n+1}=0$ to satisfy continuity. Therefore, in solving Eq. (5), the dilation term $\nabla.\mathbf{V}^{n+1}$ is put to zero to enforce the continuity equation. However, due to either limited arithmetic precision or insufficient iterations in the solution of Eq. (5), there is a residual dilation $\nabla.\mathbf{V}^{n}$ that remains as a source term in the Poisson equation which continuously reduces the dilation residue itself. This residual term takes into account the errors in the velocity field calculation due to the inexact solution of the Poisson equation in previous steps and contributes to stabilize the calculation of the numerical solution (Hirt and Harlow, 1967).

In the semi-staggered mesh, Fig. 1(a), the pressure is located at the center of the continuity control volume and both velocity components are co-located at its vertices. In principle, this mesh is ideal in the sense that it eliminates all the velocity extrapolation inherent in the strategy of the staggered mesh when adjacent to the domain boundaries. Second, it facilitates the derivation of a consistent set of boundary conditions for velocity gradients. Finally, no explicit boundary conditions for the pressure is required to solve the pressure field.

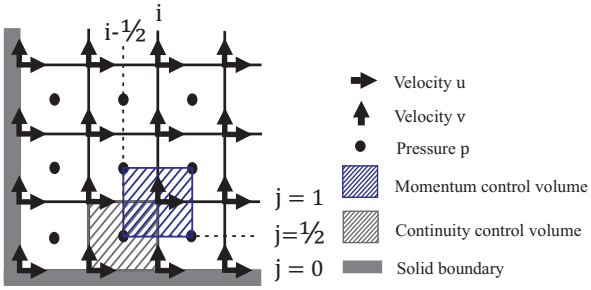

(a) Semi-staggered mesh

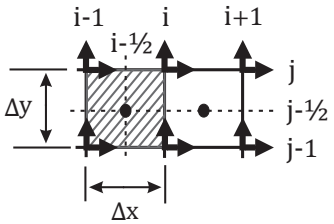

(b) Continuity control volume

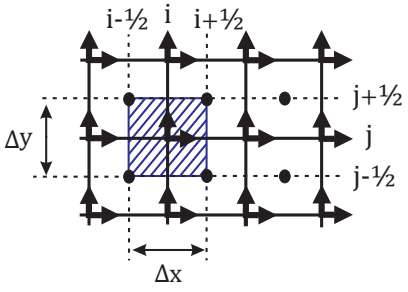

(c) Momentum control volume

Figure 1. Indexation of the dependent variables in the semi-staggered mesh.

The velocity divergent, the pressure gradient and the Laplacian pressure are expressed for the semi-staggered mesh, according to the Figs. 1(b) and 1(c), as:

$$\nabla.\mathbf{V}_{i-1/2,j-1/2}^{n}=\frac{u_{i,j}^{n}+u_{i,j-1}^{n}-u_{i-1,j}^{n}-u_{i-1,j-1}^{n}}{2\Delta x}+\frac{v_{i,j}^{n}+v_{i-1,j}^{n}-v_{i,j-1}^{n}-v_{i-1,j-1}^{n}}{2\Delta y} \tag{6}$$

$$\nabla p_{i-1/2,j-1/2}^{n}=\frac{p_{i+1/2,j+1/2}^{n}+p_{i+1/2,j-1/2}^{n}-p_{i-1/2,j+1/2}^{n}-p_{i-1/2,j-1/2}^{n}}{2\Delta x}\,\mathbf{i}$$
$$+\frac{p_{i+1/2,j+1/2}^{n}+p_{i-1/2,j+1/2}^{n}-p_{i+1/2,j-1/2}^{n}-p_{i-1/2,j-1/2}^{n}}{2\Delta y}\,\mathbf{j} \tag{7}$$

$$\nabla^2 p^n_{i-1/2,j-1/2} = -\left(\frac{1}{\Delta x^2}+\frac{1}{\Delta y^2}\right) p^n_{i-1/2,j-1/2}$$
$$+\left(\frac{0.25}{\Delta x^2}+\frac{0.25}{\Delta y^2}\right)\left(p^n_{i-3/2,j+1/2}+p^n_{i+1/2,j-3/2}+p^n_{i+1/2,j+1/2}+p^n_{i-3/2,j-3/2}\right)$$
$$+\left(\frac{0.5}{\Delta x^2}-\frac{0.5}{\Delta y^2}\right)\left(p^n_{i+1/2,j-1/2}+p^n_{i-3/2,j-1/2}-p^n_{i-1/2,j+1/2}-p^n_{i-1/2,j-3/2}\right) \quad (8)$$

The pressure equation for a control volume adjacent to a solid wall, say, the one around node $(i-{}^1\!/_2, {}^1\!/_2)$ in the Fig. 1(a), is deduced simply by using the boundary conditions imposed on the velocity field ($u^{n+1}_{i,0}$, $u^{n+1}_{i-1,0}$, $v^{n+1}_{i,0}$ and $v^{n+1}_{i-1,0}$) in the continuity equation. In doing so, all pressure nodes will be internal to the domain and no explicit pressure boundary condition will be required.

From the velocity field u^n and v^n at $t = t_n$, the calculation procedure follows the following steps: Each iteration starts by solving Eq. (5), by an iterative method, to obtain the pressure field at instant n. Then, appropriate pressure values p^n, obtained in the previous step, are substituted in Eq. (4) to explicitly calculate the velocity field at instant $n + 1$.

3. RESULTS AND DISCUSSION

A numerical method for the solution of the continuity and Navier-Stokes equations is applied to simulate laminar flows in two-dimensional symmetric channels. Due to the explicit temporal integration procedure, the time step was fixed, in each case, according to a usual heuristic procedure, such as the minimum between the advective limit $\min\{\Delta x/\mathrm{Re}, \Delta y/\mathrm{Re}\}$ obtained from the CFL condition and the diffusive limit $0.5/(1/\Delta x^2 + 1/\Delta y^2)$, multiplied by a safety factor $F = 0.5$. The root mean square (rms) of the linear momentum was adopted as the stopping criterion of the numerical solution, which should be less than 10^{-6}. The pressure Poisson equation is solved iteratively with 200 sweeps by a sub-relaxation method.

Consider a flow of an incompressible, Newtonian, viscous fluid through a flat channel with height d, which expands symmetrically, to a channel with height D, as shown in Fig. 2. In the dimensionless form of the continuity and Navier-Stokes equations, the velocity components are normalized by the average velocity $\overline{U}$ at the channel inlet, and the spatial coordinates by the upstream channel height d. Thus, in the present paper, the Reynolds number is defined as $\mathrm{Re} = \overline{U}\, d/\nu$, where ν is the kinematic viscosity.

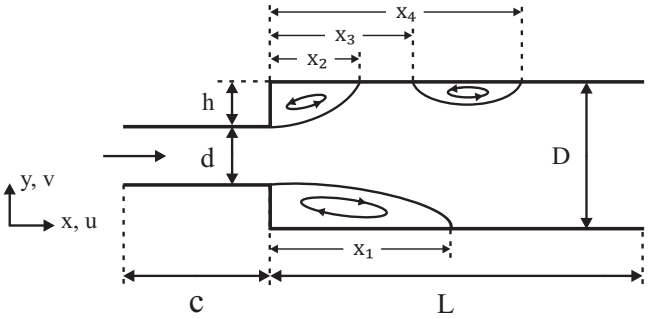

Figure 2. Sketch of symmetric channel geometry and reattachment lengths nomenclature.

The dimensions of the geometry in Fig. 2 are composed of a inlet channel height $d = 1$, a fluid inlet region with length $c = 5d$ and downstream channel length $L = 45d$, such that the fully developed parabolic flow is recovered at the channel outlet. The expansion ratio is defined as D/d, where D is the downstream channel height and d is the upstream channel height. h is the step height. All solid contours are impermeable and non-slip boundary conditions, $u = v = 0$, are imposed along the channel walls. At the domain outlet, located at $x = (c + L)$ and $0 \leq y \leq D$, the homogeneous Neumann boundary condition, $\partial u/\partial x = 0$ and $\partial v/\partial x = 0$, was assumed for the velocity components. At the inlet, a fully developed parabolic velocity profile was specified.

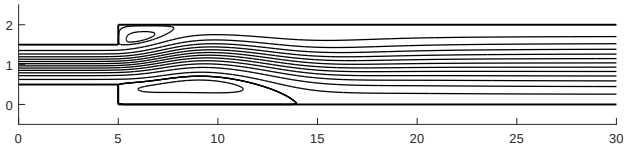

Figure 3. Streamlines for the case $\mathrm{Re} = 200$.

Uniform rectangular grids were used in numerical simulations. To assess the effect of grid resolution, a case of laminar flow at Re $= 200$ and expansion ratio 1:2 was selected. This case involves asymmetric separation, as seen from the streamlines in Fig. 3. A grid sensitivity study was performed using two grids: 150×60 and 200×80. A grid independence solution is verified in Fig. 4, comparing the skin friction distribution on the wall in two grids. The skin friction, c_f, is defined by $c_f = \tau_w/(\frac{1}{2}\rho\overline{U}^2)$, where τ_w is the wall shear stress. Both grids captured the same number of recirculation regions, and the difference in prediction of their sizes was less than 2%. The grid spacings Δx and Δy were maintained for the expansion ratio 1:3. Thus, grids of 150×90 and 200×120 were used in this case.

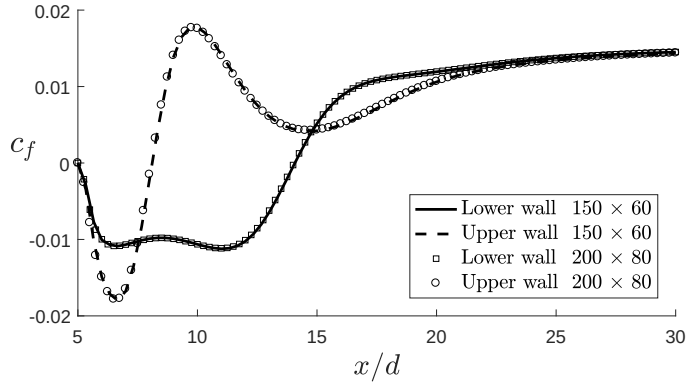

Figure 4. Verification of the grid independence solution for the case Re $= 200$.

To validate the solution method, computations were performed for Reynolds numbers Re $= 35$, 80 and 187, which are referred to as Re $= 26$, 60 and 140 in the study of Fearn *et al.* (1990). The cause of the difference is due to the different definitions used to the Reynolds number. Thus, the velocity profile measured by Fearn *et al.* (1990) are compared with the numerical results of the present paper for a expansion ratio 1:3. In Figs. 5, 6 and 7, numerical computations are represented by solid lines, whereas experimental data by circle symbols.

Figure 5 shows the comparison of velocity profiles with experimental data at various channel position for Re $= 35$.

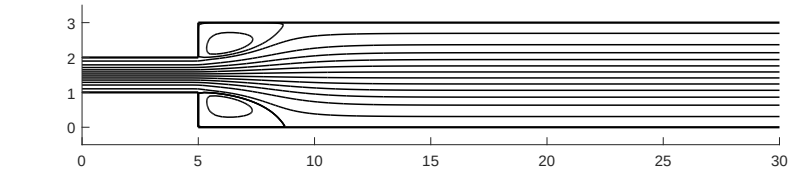

(a)

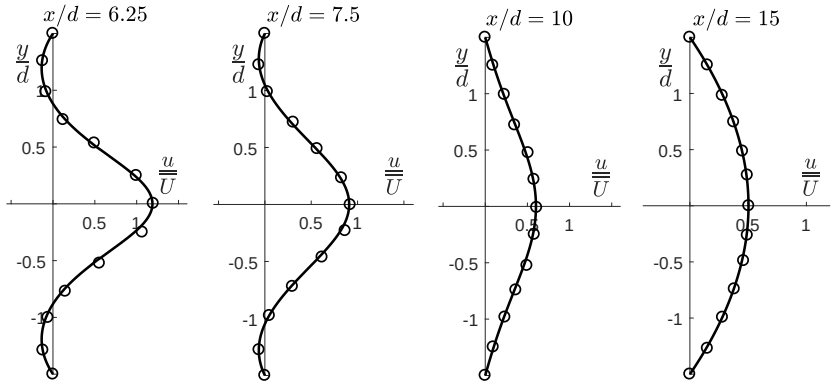

(b)

Figure 5. Comparison of velocity profiles with measurements for Re $= 35$.

Figure 5(a) shows the streamlines for Re $= 35$. Figure 5(b) shows the velocity profiles at four channel positions. In all four comparison stations, the profiles remain symmetric about to the central axis and a good agreement can be observed between the numerical and experimental results. At positions corresponding to the downstream distances $6.25d$ and $7.5d$, flow reversal within the recirculation regions is readily identifiable. The result at distance $15d$ downstream of the expansion shows that the flow profile is again parabolic.

Figure 6 shows similar information for Re $= 80$. By increasing the Reynolds number to 80, the flow becomes asymmetric with two recirculation regions of different sizes in the upper and lower walls, as illustrated by the streamlines in Fig. 6(a). Good agreement between the experimental and numerical results of the flow in this steady asymmetric regime is also shown in the series of velocity profiles in Fig. 6(b). The results at Re $= 80$ indicate that the flow retains a marked asymmetry at $x = 10d$, until it becomes parabolic again at a downstream distance of $25d$.

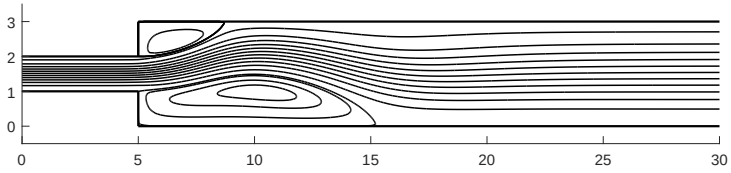

(a)

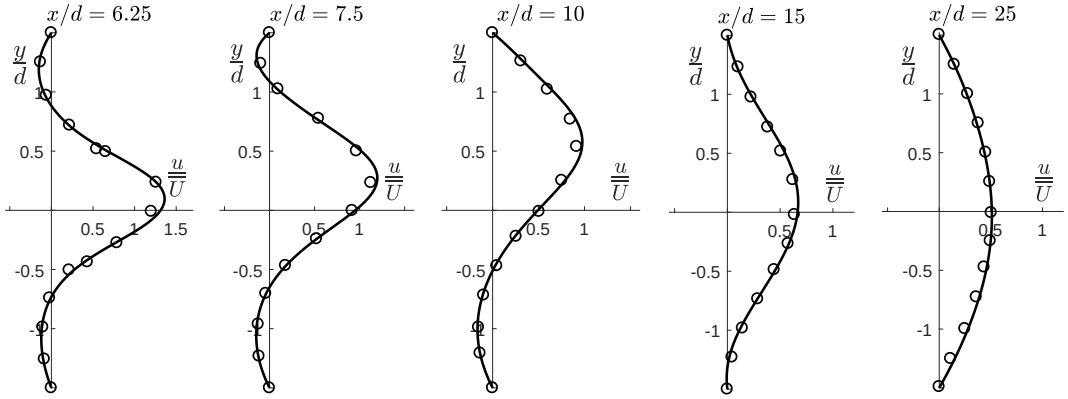

(b)

Figure 6. Comparison of velocity profiles with measurements for Re $= 80$.

A further increase in the Reynolds number to 187 results in the development of a third recirculation zone, formed on the same side of the smaller of the previous two, which is visible at station $x = 25d$. These results are presented in Fig. 7.

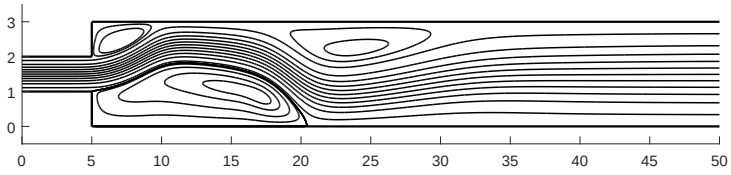

(a)

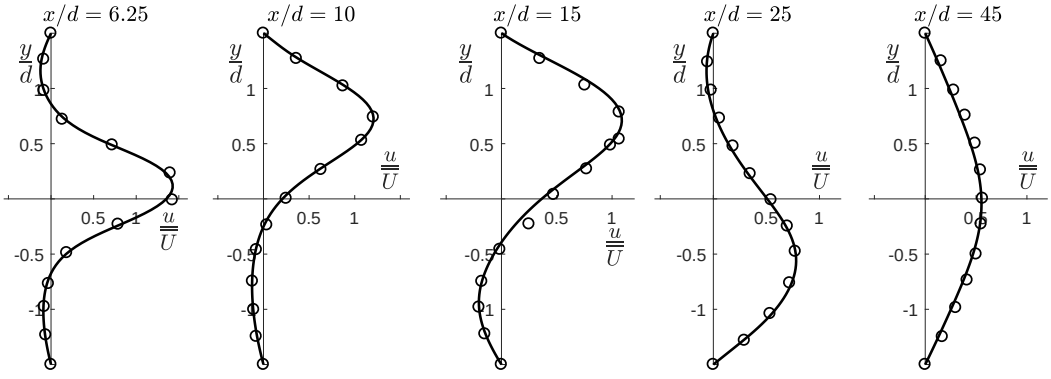

(b)

Figure 7. Comparison of velocity profiles with measurements for Re $= 187$.

In general, the calculations obtained from the numerical solutions had a good agreement with the experimental data of Fearn *et al.* (1990). The prediction of the flow field on both sides of the critical condition presented good results when compared with experimental data. This validates the solution method of the present paper, which is used in the following computations and in determining the bifurcation point of the flow.

The transition from a symmetric stable to an asymmetric flow is illustrated in the bifurcation diagram shown in Fig. 8, for an expansion ratio 1:2. In this figure, the distance between the reattachment points on the lower and upper walls (ΔX) are plotted against the Reynolds number. In the present paper, the predicted critical Reynolds number is in the range of $\mathrm{Re}_{cr} = 142$ to 143 (the exact value of the critical Reynolds number is difficult to fix due to grid resolution dependence). This interval is in accordance with the numerical predictions of Drikakis (1997) ($\mathrm{Re}_{cr} = 144$) and the stability analyzes of Shapira *et al.* (1990) ($\mathrm{Re}_{cr} = 143.3$), but is different from the value calculated by Durst *et al.* (1993) ($\mathrm{Re}_{cr} = 83.3$). Drikakis (1997), provides a possible explanation of what might have affected the calculations of Durst *et al.* (1993).

For an expansion ratio 1:3, the critical Reynolds number is in the range of $\mathrm{Re}_{cr} = 52$ to 53, having a good agreement with the results of Fearn *et al.* (1990) ($\mathrm{Re}_{cr} = 53.9$) and the bifurcation calculations of Battaglia *et al.* (1997) ($\mathrm{Re}_{cr} = 53.8$). The critical Reynolds number of the symmetry-breaking bifurcation was investigated for expansion ratios 1:2 and 1:3, and these results are compared with those of the literature in Tab. 1. It should be mentioned that, to obtain these small ranges of critical Reynolds number values, a more pronounced refinement of the grid was required close to the critical flow condition.

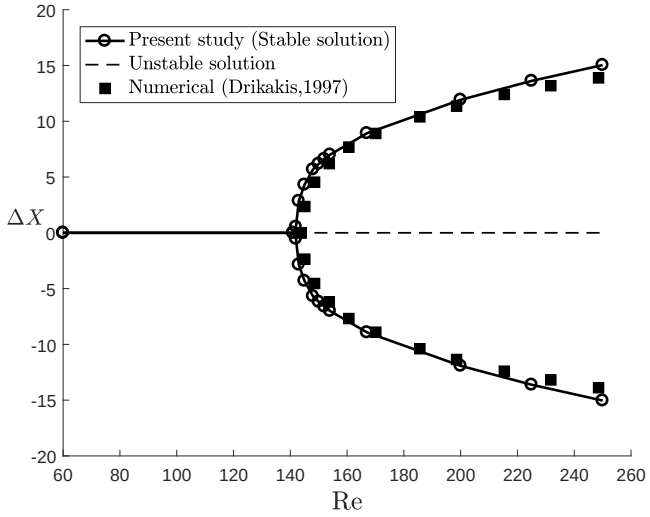

Figure 8. Bifurcation diagram for expansion ratio 1:2.

Table 1. Critical Reynolds numbers for expansion ratios 1:2 and 1:3.

Reference	Methods	Re_{cr} (ER = 1:2)	Re_{cr} (ER = 1:3)
Present study	Numerical simulation	$142 - 143$	$52 - 53$
Battaglia *et al.* (1997)	Numerical simulation	$150 - 155$	$57 - 58$
Drikakis (1997)	Numerical simulation	144	53.3
Durst *et al.* (1993)	Numerical simulation	83.3	–
Fearn *et al.* (1990)	Bifurcation analysis	–	53.9
Shapira *et al.* (1990)	Bifurcation analysis	143.3	55
Battaglia *et al.* (1997)	Bifurcation analysis	143.6	53.3
Alleborn *et al.* (1997)	Bifurcation analysis	145.3	53.3
Cherdron *et al.* (1978)	Experiments	123.3	–

The bifurcation can also be illustrated by considering how the flow reattaches to the channel walls for symmetric and asymmetric regimes. The global development of the steady flow obtained with increasing Reynolds number, can be seen in the series of images of the streamlines shown in Figs. 9(a) and 9(b) for the expansion ratios 1:2 and 1:3, respectively.

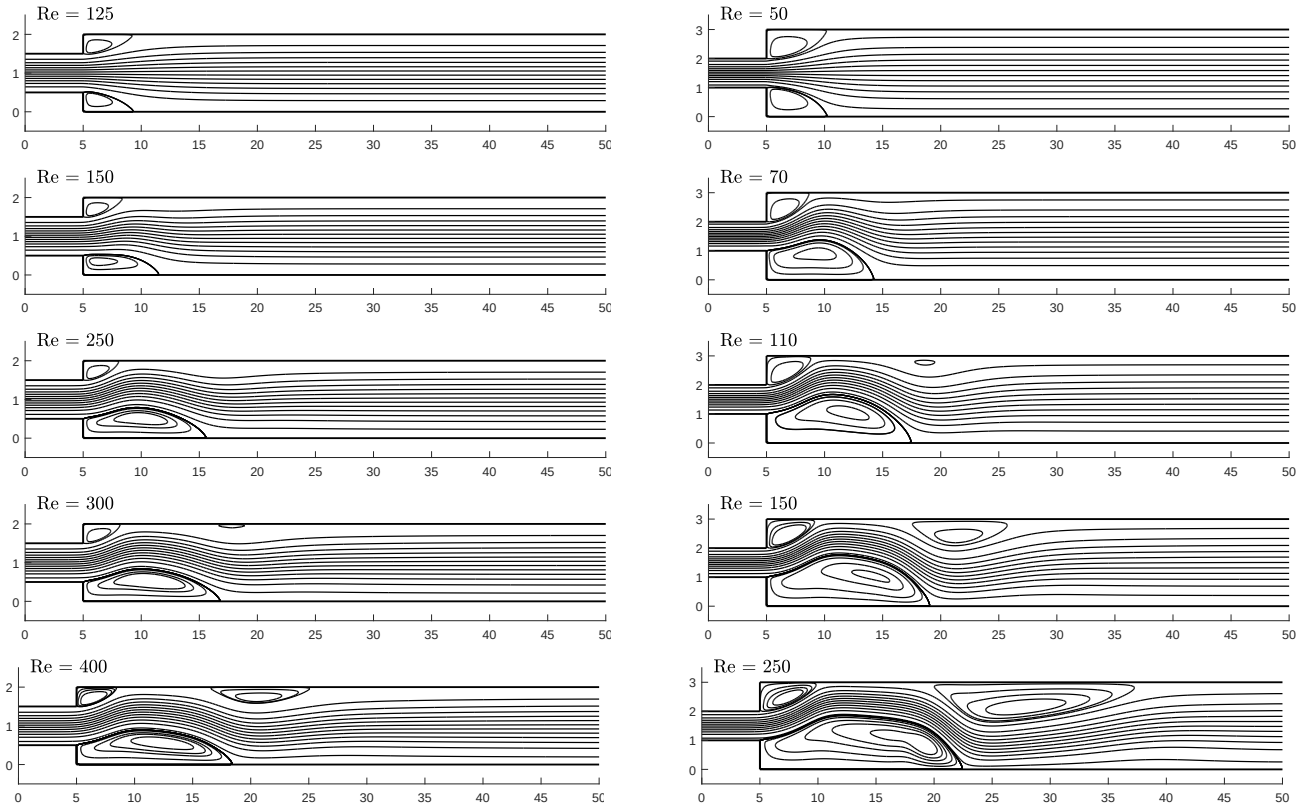

(a) Expansion ratio 1:2

(b) Expansion ratio 1:3

Figure 9. Calculated streamlines at various Reynolds numbers for expansion ratios 1:2 and 1:3.

The flow development is shown in more condensed form in Fig. 10, for expansion ratios 1:2 and 1:3, in which the recirculation region lengths are shown as a function of Reynolds number. The nomenclature of the reattachment lengths follows the definition given in Fig. 2.

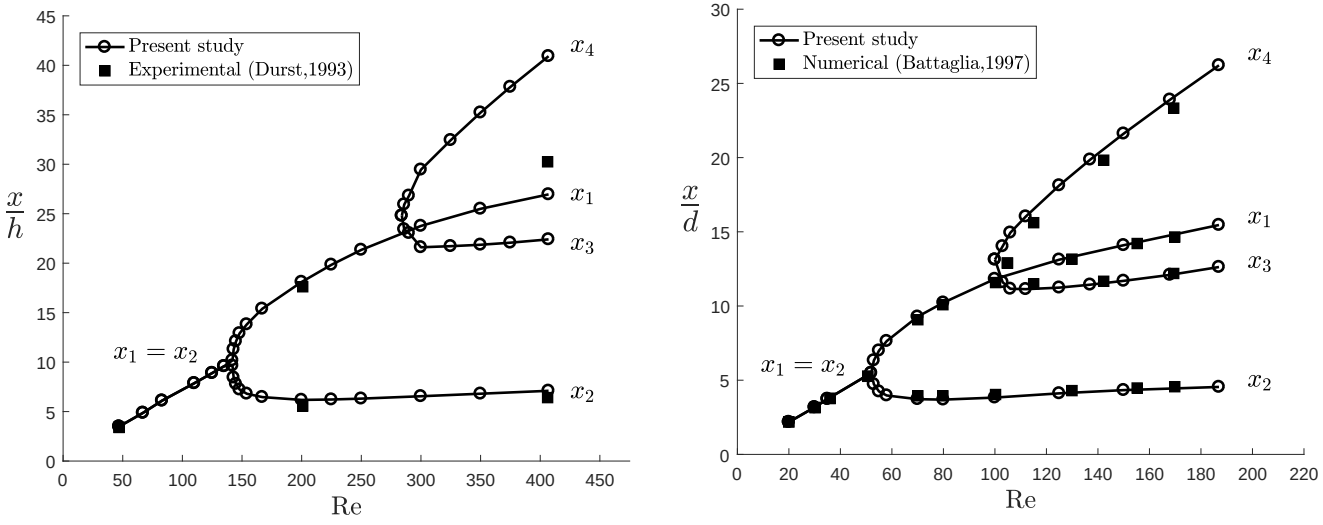

(a) Expansion ratio 1:2

(b) Expansion ratio 1:3

Figure 10. Evolution of reattachment lengths as a function of Reynolds number for expansion ratios 1:2 and 1:3.

Initially, at very low Reynolds numbers, the lengths x_1 and x_2 are equal, indicating symmetric flow. At a critical Reynolds number there is a branching that indicates asymmetric flow, for which the length x_2 remains relatively constant, while the length x_1, on the opposite channel wall, starts to increase monotonically. A third recirculation region develops further increases in the Reynolds number, represented by the lengths x_3 and x_4.

The experimental work of Durst *et al.* (1993) carried out more extensive measurements for three Reynolds numbers, namely, 47, 200 and 407, based on the definition of the present paper. The recirculation region lengths were normalized to the step height h, as shown in Fig. 10(a). This figure also indicates a good agreement between the numerical and experimental results, except for the length x_1 at Re $= 407$, which presented a value about 10.5% lower than that observed in the measurements. This result is still better than the numerical computations presented by Durst *et al.* (1993), predicting an value 18% lower than the experimental one. The third recirculation region appears near Re $= 284$, which corresponds to the lengths x_3 and x_4. Durst *et al.* (1993) mention that no attempt was made experimentally to determine the lengths of this third recirculation region.

The recirculation lengths for the expansion ratio 1:3 are compared in Fig. 10(b) with the numerical work of Battaglia *et al.* (1997). The lengths were normalized to the inlet channel height d and, in general, good agreement was obtained between the results. In this case, the third recirculation region begins to develop around Re $= 100$. Battaglia *et al.* (1997) mention that this qualitative change in flow is not associated with a bifurcation point of the Navier-Stokes equations.

Reynolds number effects on the pressure distributions were also investigated. The pressure coefficient distributions along the x coordinate at various Reynolds numbers for expansion ratios 1:2 and 1:3 are illustrated in Fig. 11. The pressure coefficient, c_p, is defined as $c_p = (p_w - p_{in})/(\frac{1}{2}\rho\overline{U}^2)$, where p_w is the pressure on the wall and p_{in} the upstream centerline pressure corresponding the maximum inlet velocity.

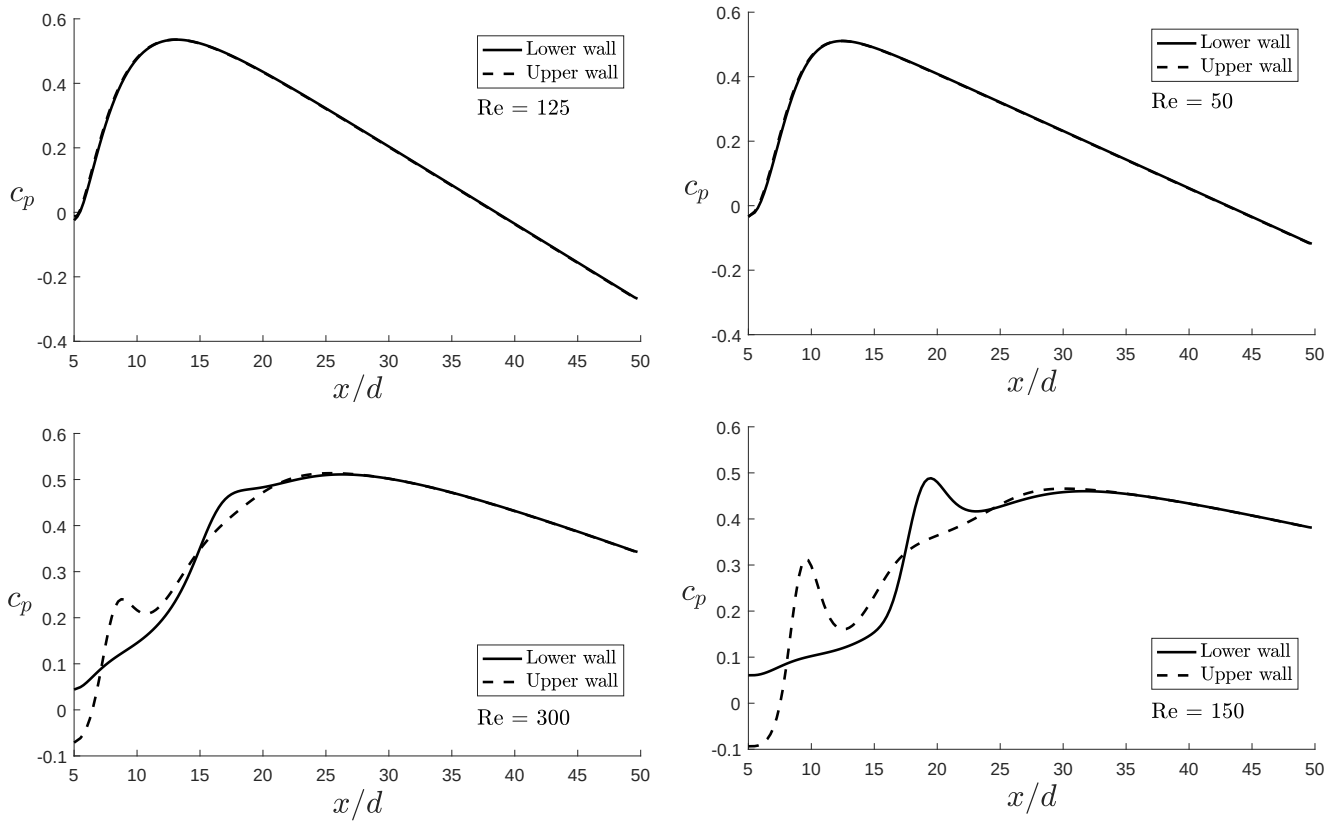

(a) Expansion ratio 1:2

(b) Expansion ratio 1:3

Figure 11. Pressure coefficient distributions at various Reynolds numbers for expansion ratios 1:2 and 1:3.

Under symmetric separation conditions, the pressure on the upper and lower walls are the same. One can see, in Fig. 11(a) for Re $= 125$ and in Fig. 11(b) for Re $= 50$, that the pressure initially increases in the channel, reaches a maximum value downstream of the expansion edge, and then gradually decreases toward the outlet. This is because of the fact that the flow returns to become fully developed. For fully developed flow, the pressure drop, caused by frictional effects, is inversely proportional to Reynolds number. Consequently, the slope of the pressure coefficient distribution for Re $= 300$ is lower than in the case Re $= 125$, for the expansion ratio 1:2. Similar behavior occurs for expansion ratio 1:3.

When flow asymmetry occurs, the pressure has different values on the upper and lower walls. For the Reynolds numbers Re $= 300$ (Fig. 11(a)) and Re $= 150$ (Fig. 11(b)), a pressure drop occurs downstream of the recirculation zone on the lower wall and downstream of the smaller recirculation zone on the upper wall, but this behavior does not occur at the third recirculation zone on the upper wall. In fact, the appearance of the pressure drop on the upper wall is due to the formation of a recirculation zone on the lower wall. In this case, the recirculation zone creates a displacement of the flow, seen from the streamlines in Fig. 9, and consequently a pressure drop on the opposite wall. However, this does not occur

downstream of a third recirculation zone on the upper wall, because the flow on the lower wall is already attached and, therefore, can not create a displacement of the flow with a pressure drop.

4. CONCLUSIONS

A numerical method for the solution of the continuity and Navier-Stokes equations that employs the Eulerian description of the flow, primitive variables on the divergent form, finite volume approach, semi-staggered mesh, UNIFAES scheme for discretization of the spatial derivatives of the advective-diffusive transport equation, explicit procedure for the temporal integration of the velocity field and Poisson equation for pressure, was successfully applied to simulate incompressible laminar flows in two-dimensional symmetric channels. The pressure equation is generally not diagonally dominant, except in the case $\Delta x = \Delta y$. Thus, it was also possible to solve the pressure equation not diagonally dominant of the semi-staggered mesh by iterative method, employing an adequate sub-relaxation factor. The final residue level of the mass conservation was approximately 10^{-11}.

Calculation of the flow field showed that the transition from a symmetric to an asymmetric flow pattern is smooth, so that the flow bifurcation is related to a symmetry-breaking instability. In this case, the numerical computations of the present paper proved satisfactory to find the critical Reynolds number, in addition to which the symmetric solution is unstable. It also has been shown that the stable asymmetric flow develops a third recirculation region, but that it is not related to an instability of the flow. The critical Reynolds number of the symmetry-breaking bifurcation was determined for expansion ratios 1:2 and 1:3. The computations have shown that the critical Reynolds number reduces when increasing the expansion ratio. The results of numerical simulations had a good agreement with experimental and numerical studies available in the literature.

5. ACKNOWLEDGMENTS

This work was conducted during a scholarship supported and financed by CAPES - Brazilian Federal Agency for Support and Evaluation of Graduate Education within the Ministry of Education of Brazil.

6. REFERENCES

Alleborn, N., Nandakumar, K., Raszillier, H. and Durst, F., 1997. "Further contributions on the two-dimensional flow in a sudden expansion". *Journal of Fluid Mechanics*, Vol. 330, pp. 169–188.

Battaglia, F., Tavener, S.J., Kulkarni, A.K. and Merkle, C.L., 1997. "Bifurcation of low reynolds number flows in symmetric channels". *AIAA Journal*, Vol. 35, No. 1, pp. 99–105.

Cherdron, W., Durst, F. and Whitelaw, J.H., 1978. "Asymmetric flows and instabilities in symmetric ducts with sudden expansions". *Journal of Fluid Mechanics*, Vol. 84, No. 01, p. 13.

Drikakis, D., 1997. "Bifurcation phenomena in incompressible sudden expansion flows". *Physics of Fluids*, Vol. 9, No. 1, pp. 76–87.

Durst, F., Melling, A. and Whitelaw, J.H., 1974. "Low reynolds number flow over a plane symmetric sudden expansion". *Journal of Fluid Mechanics*, Vol. 64, No. 01, p. 111.

Durst, F., Pereira, J.C.F. and Tropea, C., 1993. "The plane symmetric sudden-expansion flow at low reynolds numbers". *Journal of Fluid Mechanics*, Vol. 248, No. -1, p. 567.

Fearn, R.M., Mullin, T. and Cliffe, K.A., 1990. "Nonlinear flow phenomena in a symmetric sudden expansion". *Journal of Fluid Mechanics*, Vol. 211, No. -1, p. 595.

Figueiredo, J.R., 1997. "A unified finite-volume finite-differencing exponential-type scheme for convective-diffusive fluid transport equations". *Journal of the Brazilian Society of Mechanical Sciences*, Vol. 19, No. 3, pp. 371–391.

Harlow, F.H. and Welch, J.E., 1965. "Numerical calculation of time-dependent viscous incompressible flow of fluid with free surface". *Physics of Fluids*, Vol. 8, No. 12, p. 2182.

Hirt, C. and Harlow, F.H., 1967. "A general corrective procedure for the numerical solution of initial-value problems". *Journal of Computational Physics*, Vol. 2, No. 2, pp. 114–119.

Nascimento, A.H.G., Rodrigues, G.S. and Figueiredo, J.R., 2018. "Performance of finite volume discretization schemes for the convective-diffusive linear transport equation. part i: Low eigenvalue-peclet ratios". *17th Brazilian Congress of Thermal Sciences and Engineering*.

Rodrigues, G.S., Nascimento, A.H.G. and Figueiredo, J.R., 2018. "Performance of finite volume discretization schemes for the convective-diffusive linear transport equation. part ii: High eigenvalue-peclet ratios". *17th Brazilian Congress of Thermal Sciences and Engineering*.

Rodrigues, G.S., Nascimento, A.H.G. and Figueiredo, J.R., 2019a. "Performance of finite volume discretization schemes in the backward-facing step problem. part i: Stability of schemes". *25th International Congress of Mechanical Engineering*.

Rodrigues, G.S., Nascimento, A.H.G. and Figueiredo, J.R., 2019b. "Performance of finite volume discretization schemes

in the backward-facing step problem. part ii: Numerical error of schemes". *25th International Congress of Mechanical Engineering*.

Shapira, M., Degani, D. and Weihs, D., 1990. "Stability and existence of multiple solutions for viscous flow in suddenly enlarged channels". *Computers & Fluids*, Vol. 18, No. 3, pp. 239–258.

Wille, R. and Fernholz, H., 1965. "Report on the first european mechanics colloquium, on the coanda effect". *Journal of Fluid Mechanics*, Vol. 23, No. 04, p. 801.

7. RESPONSIBILITY NOTICE

The authors are the only responsible for the printed material included in this paper.